Available online at www.sciencedirect.com
ScienceDirect
Journal of Power Sources 161 (2006) 275–281
JOURNAL OF POWER SOURCES
www.elsevier.com/locate/jpowsour

CF_4 plasma treatment for preparing gas diffusion layers in membrane electrode assemblies

Yi-Hao Pai [a], Jyh-Harng Ke [b], Hsin-Fu Huang [a], Chih-Ming Lee [a], Jyh-Myng Zen [b], Fuh-Sheng Shieu [a,*]

[a] *Department of Materials Engineering, National Chung Hsing University, Taichung 402, Taiwan*
[b] *Department of Chemistry, National Chung Hsing University, Taichung 402, Taiwan*

Received 13 February 2006; received in revised form 14 March 2006; accepted 28 March 2006
Available online 11 May 2006

Abstract

The hydrophobic properties of carbon fibers improved by a CF_4 plasma treatment were used to fabricate gas diffusion layers (GDLs) for use in proton exchange membrane fuel cells. The water contact angle of the CF_4 plasma treated GDL was measured as $132.8 \pm 0.2^\circ$ at 45 °C and very few surface gas diffusion pores were either sealed or blocked by the excessive hydrophobic material residuals. Polarization measurements verified that the CF_4 plasma treated modules can indeed enhance fuel cell performance, compared to the membrane electrode assemblies (MEAs) with a non-wet-proofed GDL, 10 wt% PTFE dip-coated GDL, and commercially available GDL (10 wt% PTFE).

Keywords: Plasma surface modification; Wet-proofed gas diffusion layer; Hydrophobic property; Water management

1. Introduction

Water management in the gas diffusion layer (GDL) plays a crucial role in the research and development of proton exchange membrane fuel cells (PEMFC). In a typical PEMFC system, water transport arises from: (1) the electroosmotic drag through the electrolyte membrane [1,2], (2) the direct production from the cathodic reduction reaction [3] and (3) the condensation of water vapor from the humidified reactant feeds [3–5]. Ideally, a GDL should provide an efficient pathway for the gas reactants to be fed homogeneously and at the same time act as an effective conduit for the produced liquid water to be removed rapidly without blocking the reactant gases [4,6]. With water transport which occurs either nearby or inside the GDL, a good GDL should be therefore not only be highly conductive but also porous and wet-proofed [6,7]. An effective wet-proofing procedure determines the hydrophobic property of the porous GDL, and subsequently affects the overall power output performance of the PEMFC.

Wet-proofed GDLs are usually prepared by coating with hydrophobic materials (e.g., polytetrafluoroethylene (PTFE) [8–10] or fluorinated ethylene propylene (FEP) [11]) onto a raw GDL (such as carbon paper or carbon cloth) [6,12]. This treatment can lead to a large contact angle between liquid water and the coated GDL. The porous channels inside the wet-proofed GDL are thus less blocked or flooded by the produced liquid water [12]. However, the wet-proofing quality of the GDLs is generally determined not only by the loading of hydrophobic materials [8–11] but also by the techniques utilized to coat the wet-proofed materials onto the GDLs [10,13]. For example, power output differences were compared in the work of Lee et al. among the rolling, spraying and screen printing methods for fabricating wet-proofed GDL [13]. Paganin et al. [9] and Giorgi et al. [10] investigated the influence of PTFE loading on the GDL and found that the polarization performances of the membrane electrode assembly (MEA) tend to decline with the increase in the PTFE contents.

Although the non-intuitive decrease of the potential–current polarization is generally attributed to the GDL porosity variation as the loading of the hydrophobic material increases [9–11], Lim and Wang [11] also pointed out the surface morphology and distribution of the hydrophobic coating materials on the carbon paper or carbon cloth should not be neglected. This surface morphology and distribution problem arises from the fact that excessive liquid in hydrophobic materials may migrate (via cap-

* Corresponding author. Tel.: +886 4 228 54563; fax: +886 4 2285 7017.
E-mail address: fsshieu@dragon.nchu.edu.tw (F.-S. Shieu).

0378-7753/$ – see front matter © 2006 Elsevier B.V. All rights reserved.
doi:10.1016/j.jpowsour.2006.03.066

illary action) towards the carbon paper or carbon cloth surfaces and consequently block or seal the surface pores during the drying process of the wet-proofing procedure. The power output of the MEA then reduces considerably once a high percentage of surface pores in a single GDL are sealed. Nowadays, a homogeneous hydrophobic coating has become a challenging issue.

The present work proposes a new CF_4 plasma treatment method to effectively improve the hydrophobic property of the GDL. The idea is adapted from the radio frequency (rf) plasma treatment widely applied in polymer surface property modifications (such as adhesion, etching, grafting, penetrability and wettability) [14,15]. The surface plasma treatment does not leave excessive hydrophobic material residuals to block or seal the gas diffusion pores. In order to demonstrate the importance and significance of a "seal-free GDL (SF-GDL)" for the power output of a PEMFC, the Pt loading utilized in the electrode catalyst layer (CL) in this study was intentionally lowered to a level conventionally called "ultra-low Pt loading", e.g., 0.04–0.05 mg cm^{-2} [16–18]. The plasma treatment can modify the surface morphologies and microstructure of the wet-proofed GDL to enhance the MEA or fuel cell power output without additional usage of expensive electrocatalytic elements. Overall, the achievement of SF-GDL and ultra-low Pt loading through the CF_4 plasma treatment are remarkable.

2. Experimental

2.1. GDL preparation

Before going to the details of the GDL preparation, the principle of the radio frequency plasma treatment used in this study is briefly introduced. When rf power is applied to a gas, it is excited into the glow discharge condition through molecular oscillations and collisions. The elastic collision frequency (υ) of the gas in this condition is usually between 10^9 and 10^{11} collisions s^{-1}, which is much higher than the applied rf [19] and the electron species in the excited gas experience much more collisions during each applied field cycle [20]. Due to the glow discharge, the excited and globally neutral plasma phase containing highly reactive species, such as ions, electrons and excited molecules, originates from the mother gas. The rf power is continuously supplied so that the excited gas remains in the plasma phase. The chemical compositions and physical characteristics of the plasma are generally determined by system parameters as reported earlier [15,21].

A schematic of plasma treatment of active carbon fibers (ACF) is shown in Fig. 1. The ACFs (square carbon cloth mats with an area of 5 cm^2) were obtained from BEAM ASSOCIATE (Taiwan) and were cleaned by a reactive ion etcher system (Trion Phantom III) under the working conditions of: 25 sccm O_2 mass flow, 150 W working power, 1×10^{-3} Torr working pressure, and a 2400 s reaction time. After cleaning the ACFs, they were treated by the CF_4 plasma method with a CF_4 mass flow rate of 25 sccm, a rf power of 150 W, a working pressure of 1×10^{-3} Torr, and a reaction time of 2400 s in the reactive ion etcher system (Trion Phantom III). The CF_4 plasma treated carbon cloth mats then serve as the first set of GDL in this work. The second set of GDL used in this work was made by dip-coating method. The ACF mats were dip-coated in 10 wt% PTFE solutions, a procedure manually performed in an open beaker with a dipping time of approximately 12 s. The dip-coated carbon cloth mats were then dried in a vacuum oven at room temperature for 1 day.

2.2. Membrane electrode assembly preparation

The MEAs fabrication procedure is as follows. A Nafion® 112 (Du Pont) polymer electrolyte membrane (PEM) was first

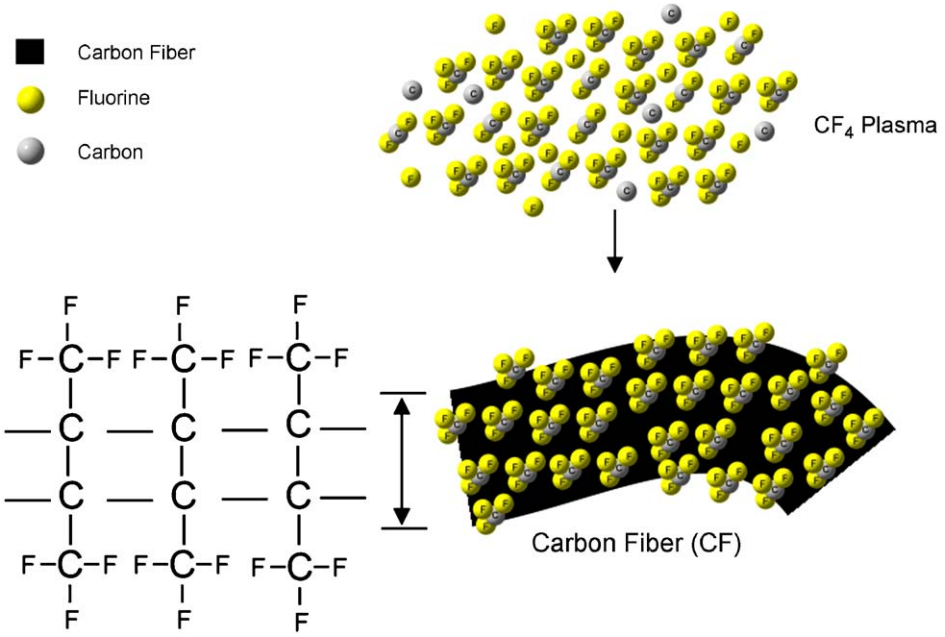

Fig. 1. Schematic diagram of the CF_4 plasma treatment on the ACFs.

immersed in 5% H_2O_2 at 80 °C for 1 h to eliminate the membrane surface impurities. The PEMs were then dipped into a 0.5 M H_2SO_4 solution at 80 °C for another hour. Lastly, the PEMs were routinely washed with boiled deionized water (D.I. water) at a temperature around 80 °C many times [22].

After pre-treatment, a 10 wt% Pt/C catalyst ink was prepared by the impregnation method [23] by using the chloroplatinic acid as the metal precursor (Seedchem) on carbon (XC-72) and the loading of the Nafion solution (Du Pont) was 5 wt%. Note that the Pt/C to Nafion ratio was based on the value reported earlier [17]. The catalyst ink was coated onto one side of the pre-treated PEMs [24,25], and dried at 80 °C and 1×10^{-2} Torr vacuum atmosphere for 1 h. The reverse side or opposite side of the membrane was treated similarly after the first side of the PEM was dried. The pre-treated PEM was sandwiched between two layers of Pt/C catalyst ink to serve as anode and cathode and the anode/PEM/cathode modules were designated as pre-MEAs. Note that the Pt loading was kept at a constant value of 0.04 mg cm^{-2} in the catalyst ink. Finally, under a vacuum atmosphere of 0.6 Torr, the GDLs and pre-MEAs were first pressed by 5 kg cm^{-2} at 60 °C for 30 s, followed by 30 kg cm^{-2} at 130 °C for 60 s [22].

2.3. Experiments on the GDL surface characterization and fuel cell polarization

The morphology, microstructure and component analyses of the GDLs (more specifically the ACF carbon cloths) were studied by JEOL 6700F SEM, Zeiss 902 A TEM and energy dispersive X-ray spectroscopy (EDXS). The liquid water contact angle (WCA) at the surface of the GDL was measured by the sessile-drop method using a contact angle system FTA 200 (ACIL & First Ten Angstroms Inc.) at 45 ± 0.4 °C. Four samples with at least three spots per GDL were measured. The electrical resistivity (R) of the ACFs was measured by an Agilent 16451B dielectric test fixture at 0.2 kgf cm^{-2}.

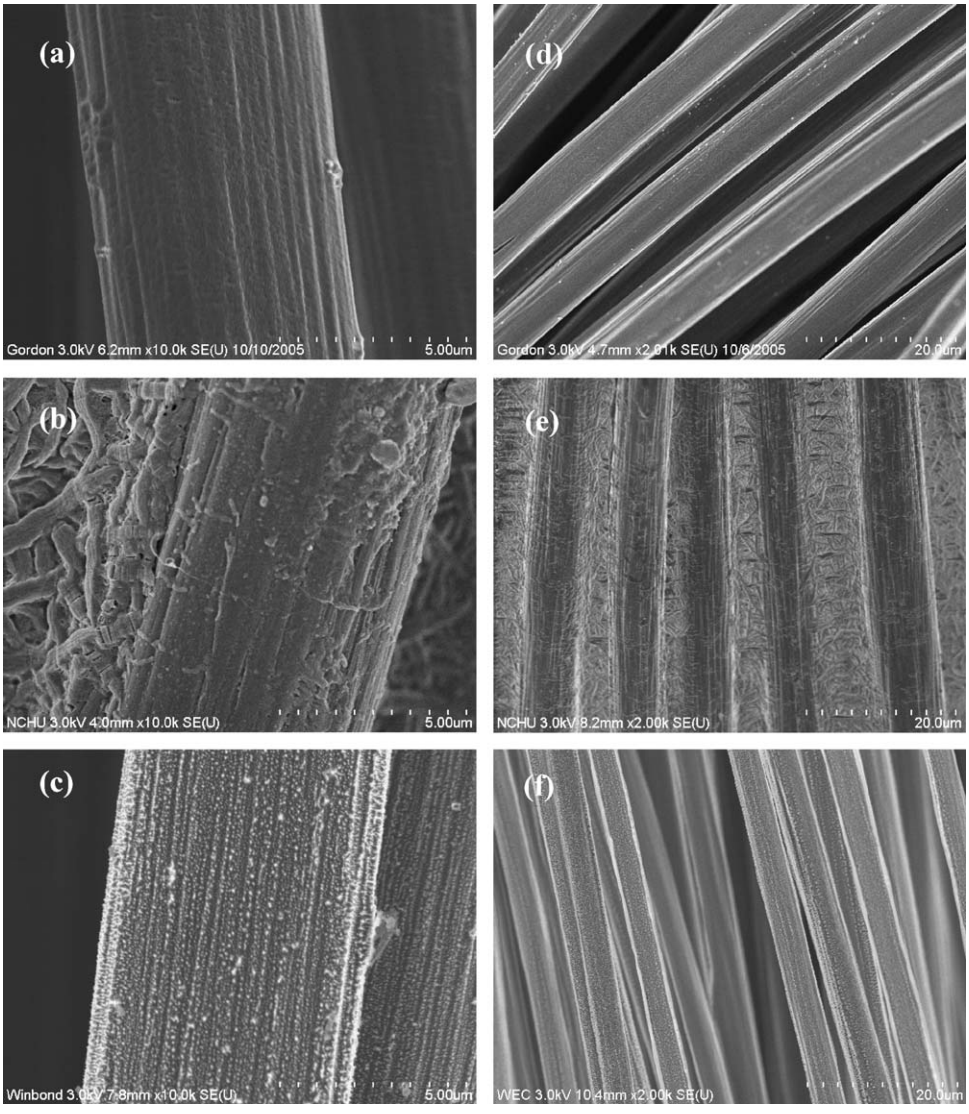

Fig. 2. Electron microscopic images of the non-treated (a and d), 10 wt% PTFE dip-coating treated (b and e) and CF_4 plasma treated wet-proofed (c and f) ACF surfaces. (a–c) At high resolution and (d–f) at low resolution.

The crystalline phase analyses of the catalyst ink layers were done by comparing the selected area diffraction (Zeiss 902 A TEM, SAD) patterns and X-ray diffraction (MAC MXT III, XRD) of the Pt/C catalysts to those of the standard compounds documented in the JCPDS [22]. The MEA polarization curves were measured by a FUEL CELL SYSTEM (BEAM ASSOCIATE CO., LTD) with the reactant streams being kept at a water vapor saturation temperature of 60 °C, a back pressure of 10 psi and a flow rate of 100 sccm. Usually, in fuel cell systems the cell operating temperature is kept higher then water vapor saturation temperature [26]. In our previous work, the operating temperature inside the MEAs was kept at 45 °C to control the water moiety from leaching out of the MEA [22]. In this work, to emphasize the excellent hydrophobic property of the GDL after the CF_4 plasma treatment, the vapor saturation temperature was intentionally set at 60 °C that is 15 °C higher than the fuel cell temperature.

3. Results and discussion

3.1. Characterization of the gas diffusion layers

Fig. 2 shows the electron microscopy of the non-treated (a and d), 10 wt% PTFE dip-coating treated (b and e) and CF_4 plasma treated wet-proofed (c and f) ACF surfaces. As can be seen, the dip-coated PTFE polymer did not have an even and homogeneous distribution on the ACF surfaces (Fig. 2b). Moreover, almost all of the gas diffusion pores next to the cylindrical carbon single fibers were either covered or sealed by the hydrophobic polymer material. This result is very different from non-treated and CF_4 plasma treated conditions (Fig. 2a and c). The excessive PTFE content is thus not favorable as it may hinder gas diffusion and water removal processes [11]. Despite similar morphologies, additional homogeneously distributed white spots were observed on the CF_4 plasma treated wet-proofed ACF surfaces, as shown in Fig. 2c. The white spots actually reflected the formation of some low resistivity spots originating from the fluorine molecules and CF_3^+ hydrophobic functional groups implanted onto the carbon fiber via the CF_4 plasma treatment. The EDXS surface analysis diagram (Fig. 3) further supports the predication that the homogeneously distributed white spots indeed came from the CF_4 plasma treatment. Most importantly, the fluorine contents can largely improve hydrophobic properties of the CF_4 plasma treated ACFs.

Fig. 4 shows the results observed from the sessile-drop tests for the processed ACFs (i.e., GDLs). The water contact angles (WCA) for the 10 wt% PTFE dip-coated ACFs and CF_4 plasma treated ACFs were measured as $128.4 \pm 0.2^\circ$ and $132.8 \pm 0.2^\circ$, respectively. Meanwhile, due to the high hydrophilicity of the non-treated case, the WCA cannot be measured in this study. Again, these results are quite consistent with the above observations. The inner electrical resistivity (i.e., through-plane conductivity) values measured were $R = 0.5\ \Omega$ for the non-treated (non-wet-proofed), $R = 0.49\ \Omega$ for the 10 wt% PTFE dip-coated (wet-proofed), and $R = 0.45\ \Omega$ for the CF_4 plasma treated (wet-proofed) ACFs. Although the CF_4 plasma treated ACFs had a slightly lower electrical resistivity, the difference in the electrical resistivity among the three conditions is not obvious.

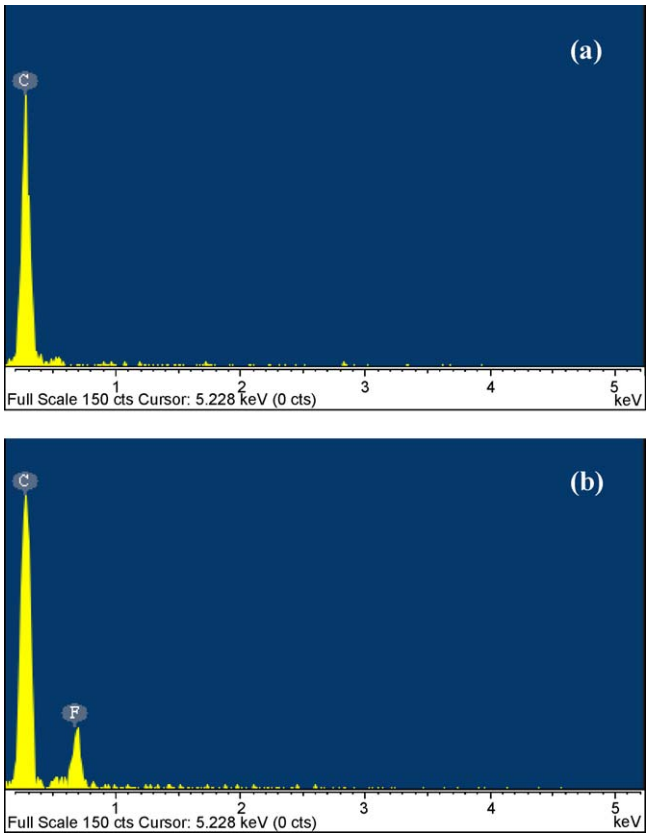

Fig. 3. The EDXS surface component analysis diagram for non-treated (a) and the CF_4 plasma treated (b) ACFs.

Overall, the CF_4 plasma treated ACFs (or GDLs) can attain a desirable hydrophobic property and a slightly reduced electrical resistance without having the surface gas diffusion pores sealed or blocked by excessive hydrophobic material residuals. This result in turn suggests that the gaseous reactants are likely to have a better access to the inner electrode catalyst layers where the primary reactions proceed. The polarization curves at high current densities are likely to preserve a higher cell voltage since the material diffusion effects are dominant in this current density region. The polarization results from the MEA test representing the overall performances for the three different categories will be discussed later. Various GDLs (i.e., ACFs) and related MEAs from local commercial merchandise (BEAM ASSOCIATE CO., Ltd., Taiwan) will also be compared. Emphasis will be placed on the cell voltages and power densities at high current densities (for ultra-low Pt loading conditions) at which the performance outputs are generally determined by material diffusion effectiveness.

3.2. Microstructure and crystal structure of the Pt/C catalysts

Fig. 5a illustrates the bright field morphology of the 10 wt% Pt/C catalyst ink material prepared by the impregnation method. As can be seen, the Pt and carbon appear in different contrast

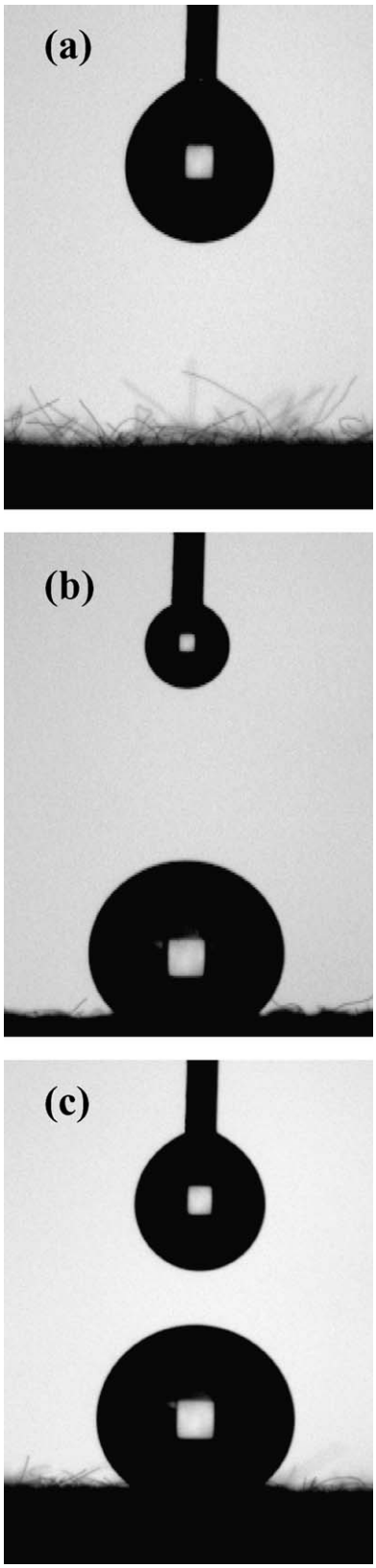

Fig. 4. Sessile-drop test for the (a) non-treated, (b) 10 wt% PTFE dip-coated and (c) CF_4 plasma treated ACFs.

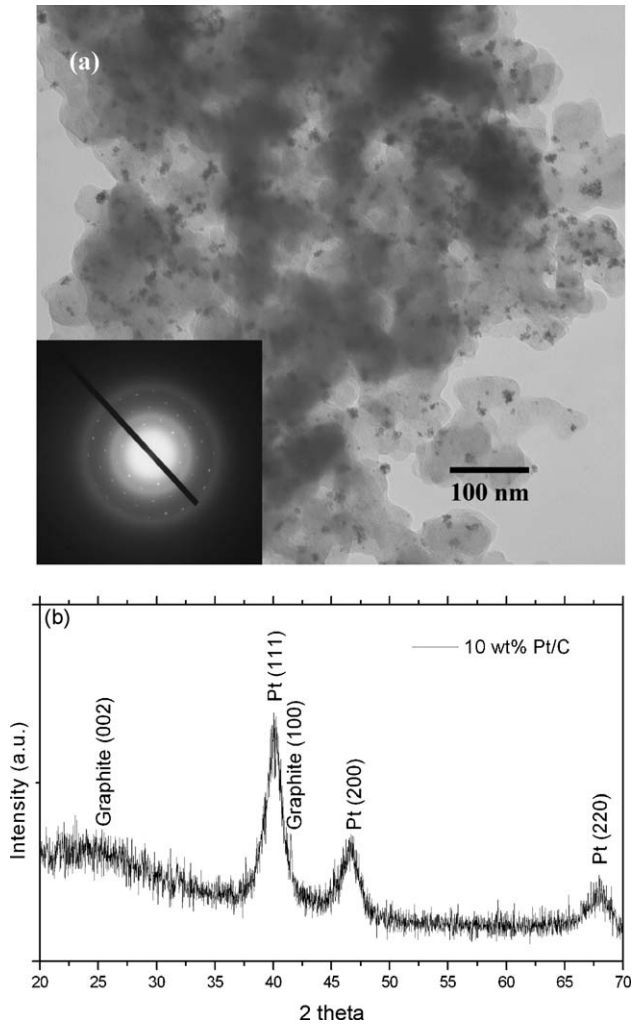

Fig. 5. The bright field morphology (a) and the X-ray diffraction diagram (b) of the Pt/C catalyst.

levels. According to the literature [27], it is expected that the high-*Z* regions (i.e., high mass regions) may scatter more electrons than the low-*Z* regions of a given sample having a constant thickness throughout. Therefore, the electron scattering from the Pt contents causes the Pt regions or high-*Z* regions on the sample to exhibit a higher contrast, and vice versa from the carbon contents. Fig. 5a also reveals a homogeneous Pt particle (average particle diameter: 5 nm) distribution on the carbon support for the Pt/C catalyst material prepared from the impregnation method. From the obtained SAD patterns, the *d* spacing was measured as 2.265 Å for the (1 1 1) reflection of the Pt phase [22]. X-ray diffraction diagram (XRD) of the Pt/C catalyst material was also obtained for crystal structure analysis (Fig. 5b). In sum, both the SAD and XRD results clearly indicate an amorphous structure of the carbon carriers.

3.3. Polarization and power density testing

Fig. 6 shows the polarization results with a 10 psi back pressure for various groups of MEAs chosen in this study. With an open circuit voltage (OCV) of 0.82 V and a reversible poten-

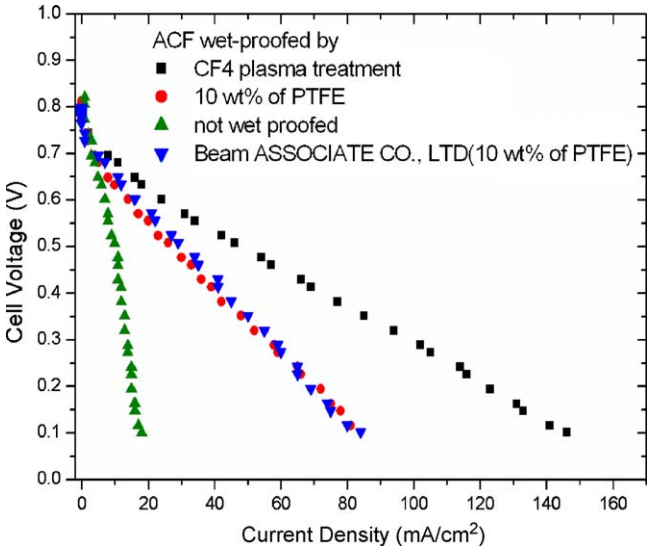

Fig. 6. The polarization results with a 10 psi back pressure for the four groups of MEAs studied. Green curve (triangle dotted), red curve (circle dotted), blue curve (upside-down triangle dotted), black curve (square dotted) represents the MEAs with untreated, 10 wt% PTFE dip-coated, BEAM and CF_4 plasma treated ACFs, respectively. All MEAs used in the test has a Pt loading of ~0.04 mg cm^{-2}.

tial of 1.23 V, the ohmic polarization ranges of the four MEA groups were compared. We found that the MEAs with CF_4 plasma treated ACFs had the widest ohmic polarization range of 15–130 mA cm^{-2}. Whereas, the ohmic range of the MEAs with 10 wt% PETF dip-coated ACFs and commercial BEAM ACFs was generally the same (i.e., 10–80 mA cm^{-2}). The narrowest ohmic polarization range of 15–18 mA cm^{-2} was observed on the MEAs with non-wet-proofed ACFs. The observed trend of the ohmic polarization behavior is consistent with the previously reported results [11,13] and demonstrates how the power output is either cut-off or shortened when liquid water distribution in the MEAs is not well managed.

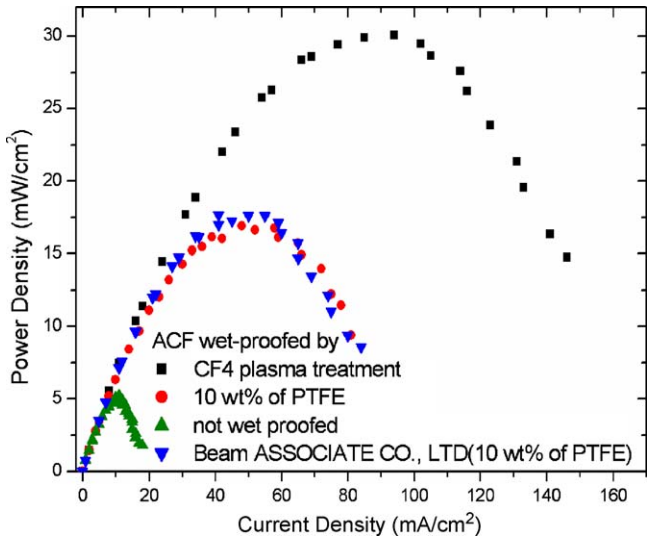

Fig. 7. The power density to current density diagram with a 10 psi back pressure for the four groups of MEAs studied. Others are the same as in Fig. 6.

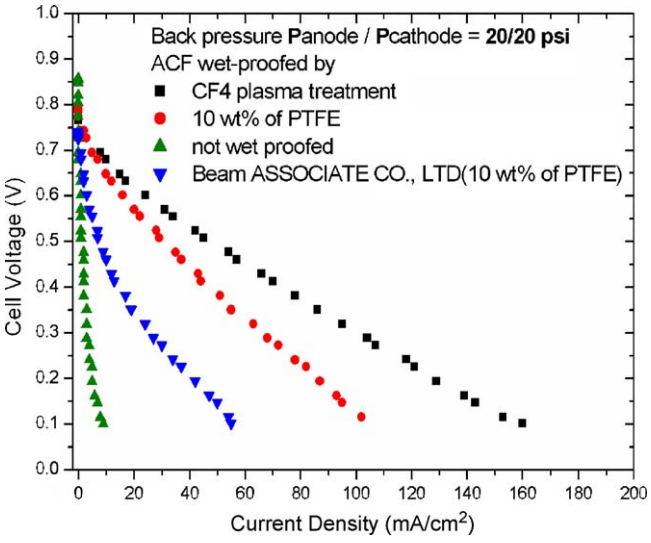

Fig. 8. The polarization results with a 20 psi back pressure for the four groups of MEAs studied. Others are the same as in Fig. 6.

Finally, the power density to current density diagram (*P–I* plot) with a 10 psi back pressure is given in Fig. 7. Again, for ultra-low Pt loading conditions, the CF_4 plasma treated MEAs shows an optimal power output of 30 mW cm^{-2} with a current density of 90 mA cm^{-2}. Note that the values are far greater than those (17.5 mW cm^{-2}, 50 mA cm^{-2}) for the 10 wt% PTFE dip-coated and commercial BEAM MEAs. At low current densities, the loss is generally due to a very poor catalyst layer, a very high protonic resistance in the ionomer due to dehydration, or a very poor contact between the cell elements, such as between catalyst layer and GDL. Only at much higher current densities, the polarization curves start to be affected by mass transport limitations of which GDLs are responsible. Figs. 8 and 9 show the polarization results and *P–I* plot with a 20 psi back pressure for various groups of MEAs chosen in this study. As can be seen, the results at much higher current densities validate the excellent

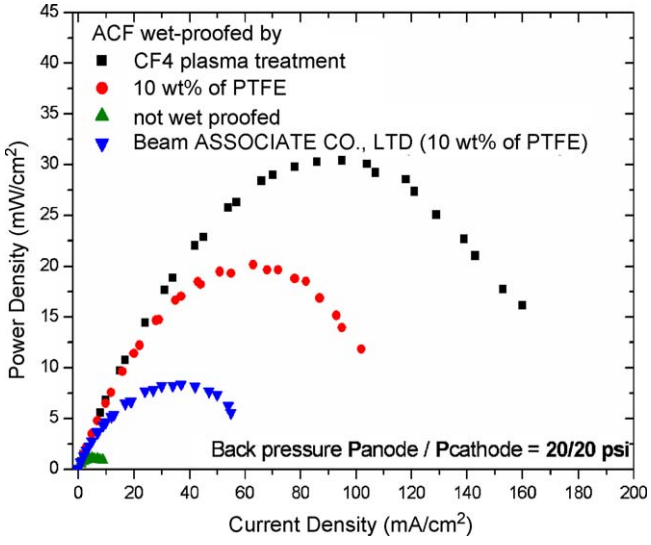

Fig. 9. The power density to current density diagram with a 20 psi back pressure for the four groups of MEAs studied. Others are the same as in Fig. 6.

property of the GDL after the CF_4 plasma treatment in fuel cell performance.

4. Conclusion

Hydrophobic properties of the ACFs (or GDLs) were effectively improved by the CF_4 plasma treatment. Surface morphologies of the non-wet-proofed ACFs, the 10 wt% PTFE dip-coated ACFs and the CF_4 plasma treated ACFs indicated that the surface gas diffusion pores of the CF_4 plasma treated ACFs were apparently less sealed or blocked by excessive hydrophobic material residuals. Water contact angles (at 45 °C) of the CF_4 plasma treated ACFs and the 10 wt% PTFE dip-coated ACFs were measured to be $132.8 \pm 0.2^\circ$ and $128.4 \pm 0.2^\circ$, respectively. Polarization and power density measurements were compared for four cases: the MEAs with non-wet-proofed ACFs, the MEAs with 10 wt% PTFE dip-coated ACFs, the MEAs with commercially fabricated ACFs (10 wt% PTFE) and the MEAs with CF_4 plasma treated ACFs. The results showed that the CF_4 plasma treated modules had the best performance among the four cases compared in the present study. Future work will be conducted to compare the CF_4 plasma treatment with other hydrophobic material coating methods, such as rolling, spraying, screen printing, etc.

Acknowledgements

The work is financially supported by the National Science Council (NSC) through grants NSC-093-2218-E-005-040 and NSC-094-2218-E-005-007.

References

[1] G. Karimi, X. Li, J. Power Sources 140 (2005) 1.
[2] X. Ren, S. Gottesfeld, J. Electrochem. Soc. 148 (2001) A87.
[3] U. Pasaogullari, C.Y. Wang, J. Electrochem. Soc. 151 (2004) A399.
[4] N. Djilali, D. Lu, Int. J. Therm. Sci. 41 (2002) 29.
[5] J. Chen, T. Matsuura, M. Hori, J. Power Sources 131 (2004) 155.
[6] S. Litster, G. McLean, J. Power Sources 130 (2004) 61.
[7] F. Barbir, PEM Fuel Cells: Theory and Practice, Elsevier Academic Press, San Diego, 2005, p. 93.
[8] D. Bevers, R. Rogers, M. von Bradke, J. Power Sources 63 (1996) 193.
[9] V.A. Paganin, E.A. Ticianelli, E.R. Gonzalez, J. Appl. Electrochem. 26 (1996) 297.
[10] L. Giorgi, E. Antolini, A. Pozio, E. Passalacqua, Electrochim. Acta 43 (1998) 3675.
[11] C. Lim, C.Y. Wang, Electrochim. Acta 49 (2004) 4149.
[12] J. Benziger, J. Nehlsen, D. Blackwell, T. Brennan, J. Itescu, J. Membr. Sci. 261 (2005) 98.
[13] H.K. Lee, J.H. Park, D.Y. Kim, T.H. Lee, J. Power Sources 131 (2004) 200.
[14] D. Barton, J.W. Bradley, D.A. Steele, R.D. Short, J. Phys. Chem. B 103 (1999) 4423.
[15] C. Riccardia, R. Barnia, E. Sellib, G. Mazzoneb, M.R. Massafrac, B. Marcandallic, G. Poletti, Appl. Surf. Sci. 211 (2003) 386.
[16] R. O'Hayre, S.J. Lee, S.W. Cha, F.B. Prinz, J. Power Sources 109 (2002) 483.
[17] L. Xiong, A. Manthiram, Electrochim. Acta 50 (2005) 3200.
[18] D. Gruber, N. Ponath, J. Muller, Electrochim. Acta 51 (2005) 701.
[19] R.F. Baddour, R.S. Timmins (Eds.), The Application of Plasmas to Chemical Processing, MIT Press, Cambridge, MA, 1967.
[20] A. Grill, Cold Plasma in Materials Fabrication, Institute of Electrical and Electronics Engineers, Inc., New York, 1994, pp. 24–45.
[21] M. Strobel, C. Lyons, K.L. Mittal (Eds.), Plasma Surface Modifications of Polymers: Relevance to Adhesion, VSP, Utrecht, 1994.
[22] Y.H. Pai, H.F. Huang, Y.C. Chang, C.C. Chou, F.S. Shieu, J. Power Sources 159 (2006) 878–884.
[23] S.R. de Miguel, J.I. Vilella, E.L. Jablonski, O.A. Scelza, C. Salinas-Martinez de Lecea, A. Linares-Solano, Appl. Catal. A-Gen. 232 (2002) 237.
[24] M. Wilson, S. Gottesfeld, J. Electrochem. Soc. 139 (1992) 28.
[25] Y.G. Chun, C.S. kim, D.H. Peck, D.R. Shim, J. Power Sources 71 (1998) 174.
[26] Z. Qi, A. Kaufman, J. Power Sources 113 (2003) 37.
[27] D.B. Williams, C.B. Carter, Transmission Electron Microscopy, Plenum, New York, 1996, pp. 351–354.